JOURNAL OF MATERIALS SCIENCE 14 (1979) 33–48

Grain boundaries and ionic conduction in sodium beta alumina

LUTGARD C. De JONGHE*
Department of Materials Science and Engineering, Cornell University, Ithaca, New York 14853, USA

Grain boundary morphology and structure has been examined by means of transmission electron microscope lattice imaging, and a plausible correlation is advanced between the grain boundary structure and its transgranular ionic resistivity and capacitance. The geometrical aspects and resistance of the grain boundaries depend on whether or not dislocations with a b = 1 spinel block can accommodate the misorientation. Such dislocations are shown to exist in a wide range of grain boundaries. The wide spread in grain boundary structure and the complexity of the microstructure, making parallel current path considerations necessary, can account qualitatively for the deviation from the ideal Maxwell dispersive behaviour. However, a physically relevant interpretation of equivalent circuit parameters determined from dispersive type measurements seems not justified. Several model circuits are used to illustrate the interpretational difficulties. The structure and effects of intergranular phases also have been studied and are discussed.

1. Introduction

Sodium beta aluminas exhibit unusual ionic conductivity properties making them useful as solid electrolytes. Even in polycrystalline form ionic resistivities at 300° C can be as low as 3 to 5 Ω cm for β'' aluminas [1], and 20 to 30 Ω cm for β aluminas [2]. Sodium conduction takes place exclusively in basal planes of these crystals. These "conduction planes" are spaced 11.3 Å apart by non-conducting spinel blocks. The conduction anisotropy has not been measured accurately; it is approximately 10^{15} at 300° C [3], so that ionic conduction in the [c] direction, normal to the conduction planes, is totally negligible. The material is a wide band gap electronic insulator (~ 4 eV) [4]. During d.c. ionic conduction in the polycrystalline solid electrolytes, the sodium ions must be transported through grain boundaries. It has been demonstrated that grain boundaries in this material are regions of high local resistance, so that they can be considered, in the simplest interpretation, as partially blocking electrodes [5]. One may suspect that the ionic resistivity for intergranular transport depends significantly on the detailed grain boundary structure. Also, since the crystals have such high conduction anisotropy, one should suspect that the solid electrolyte conduction properties are susceptible to microstructural features such as grain size and grain morphology.

In this paper some structural aspects of sodium beta alumina grain boundaries are examined and a general relationship between grain boundary resistivity, grain boundary capacitance, and structure is proposed. Furthermore, the tenuous relationship between microstructure and detailed interpretation of a.c. conductivity measurements such as complex admittance or impedance dispersion is explored. It will become evident that the dispersive method [6] does not yield data that are of fundamental significance for polycrystals. Rather, it provides an engineering correlation between microstructure and ionic conductive properties; this by itself is, of course, quite valuable.

* Now at: Materials and Molecular Research Division, Lawrence Berkeley Laboratory, University of California, Berkeley, California 94720, USA.

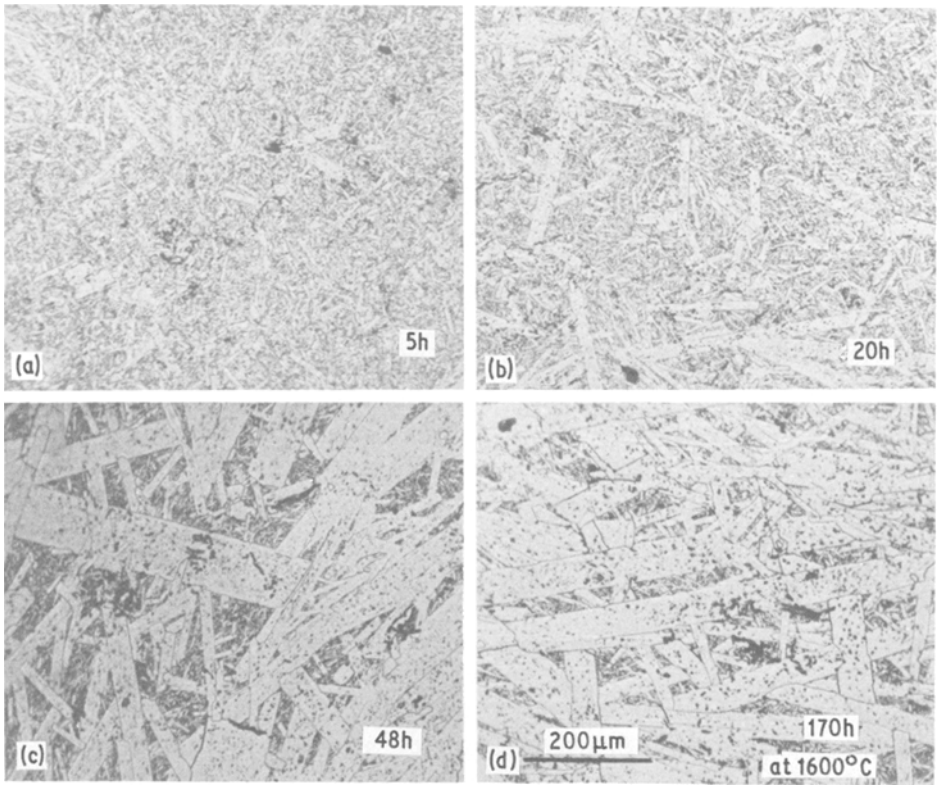

Figure 1 Microstructures of sodium beta alumina after post-annealing at 1600° C packed in β-alumina powder. (a) 5 h; (b) 20 h; (c) 48 h; (d) 170 h. Note the strong bimodal texture. After 170 h at 1600° C the sample consists of large, plate-like grains with an aspect ratio of about 10:1 with small amounts of small grain size material in isolated pockets.

2. Experimental observations

2.1. Grain growth

To establish the degree to which microstructure and grain size influence the conductive properties, grain growth experiments were carried out at 1600° C. The polycrystalline samples were annealed for up to 175 h, packed in β-alumina powder and enclosed in an α-alumina crucible. The resulting microstructures are shown in Fig. 1. Clearly, at this temperature, abnormal grain growth is extensive, leading eventually to a microstructure consisting of very large grains, with pockets of small grains trapped between them. The main difference between the initial and the final microstructures is that the aspect ratio of the large grains is about 10:1 while for the small grain size fraction it is about 3:1. The evolution of the small grain size fraction is shown in Fig. 2. After 175 h at 1600° C, the microstructural situation can thus be summarized as in Fig. 3. Essentially, one has transformed a microstructure with an average largest grain dimension of ~ 5 μm to a microstructure with an average largest grain dimension of 500 μm with a concurrent increase in the aspect ratio. By dispersive techniques discussed in Section 3 one can measure the extrapolated d.c. resistance of the samples at 75° C, where the grain boundary resistivity can be shown to be approximately 90% of the total resistivity. One would thus expect a resistivity drop of about a factor of 100 after 175 h of annealing. The measured values are shown in Fig. 4. Clearly, although the time dependence of R is approximately $R \propto t^{1/2}$ the resistivity does not drop by the expected amount and R is not proportional to the average grain dimension. Only a factor of about 10 is involved. This is an indication that the dispersive techniques may not simply characterize an average grain boundary resistivity, but perhaps involve in some way part of the bulk of the grains as well. Similar problems arise in the interpretation of Na-tracer diffusion data [7]. It should be noted that our findings do not agree with the conclusions of Virkar and Gordon [8] on grain size effects in β″-aluminas. The nature of this discrepancy is not fully under-

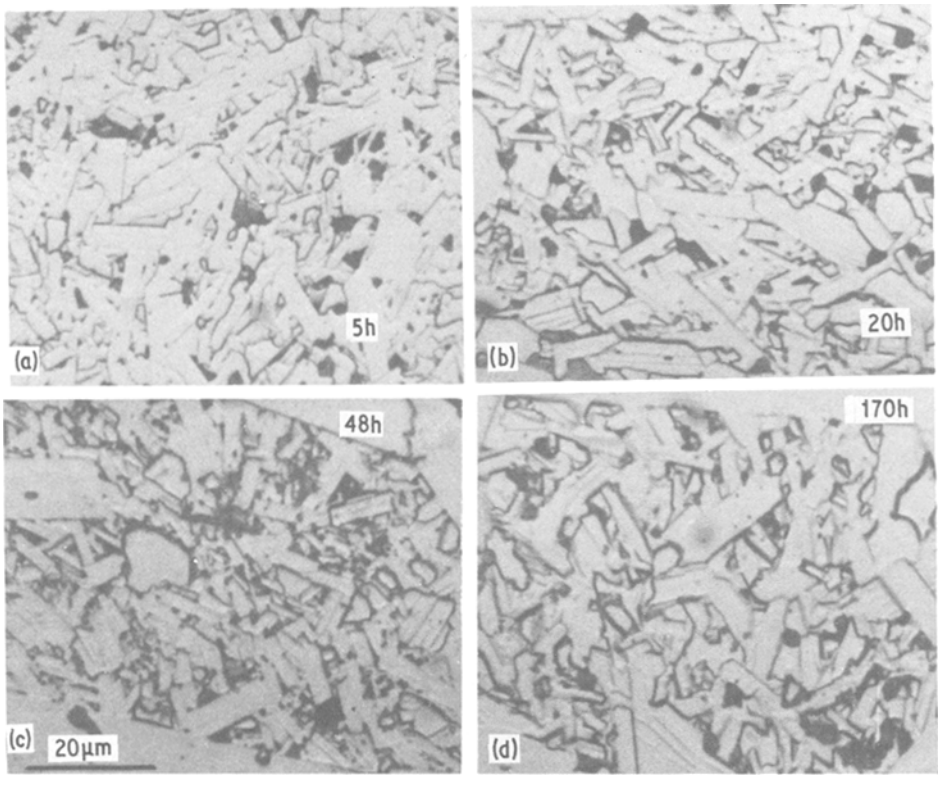

Figure 2 Microstructural evolution of small grain size fraction of sample shown in Fig. 1. The aspect ratio remains about 3 : 1, (a) 5 h; (b) 20 h; (c) 48 h; and (d) 170 h at 1600° C.

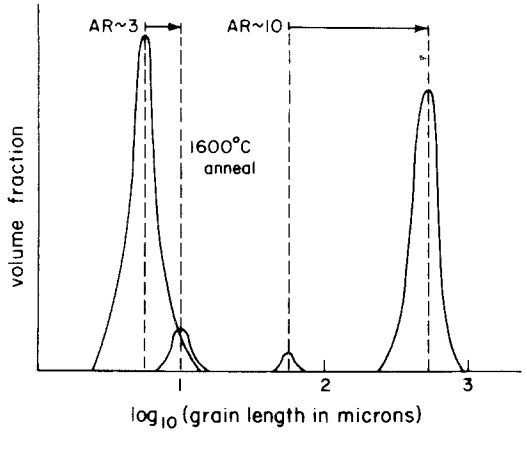

Figure 3 Qualitative comparison of initial and final (170 h at 1100° C) microstructures of sample shown in Fig. 1.

stood at present; it may reside in the differences in grain morphology and microstructures resulting from the different annealing treatments.

In what follows arguments are advanced for the presence of a wide range of grain boundary resistances making it necessary to incorporate, in principle, parallel current paths in the equivalent circuit description of the solid electrolyte. Qualitatively, the multitude of alternate paths can partly account for the observed a.c. dispersive behaviour. Although there has been extensive work in the area of heterogeneous dielectrics [9], development of a quantitative theory, taking fully into account the microstructural complexities of this non-homogeneous, microscopically anisotropic dielectric seems, at present, a difficult if not impossible task.

The a.c. measurements do maintain their value in providing reproducible correlations between microstructure and ionic conductive values. Fundamentally significant transport information about grain boundaries such as activation energy or resistivity distributions cannot, however, be extracted from dispersive measurements except in hypothetical or in simple situations such as single boundaries in welded bicrystals*.

2.2. Grain boundary structures

2.2.1. Extreme cases

Fig. 5 shows a typical microstructure of fine grained β–β'' alumina, with a 300° C d.c. ionic

*Such experiments have been initiated in our laboratory.

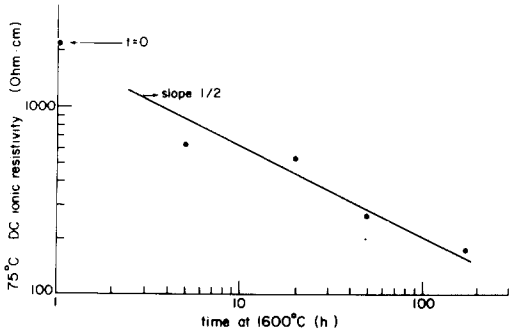

Figure 4 D.c. specific ionic resistivity at 70° C as a function of post-annealing time at 1600° C.

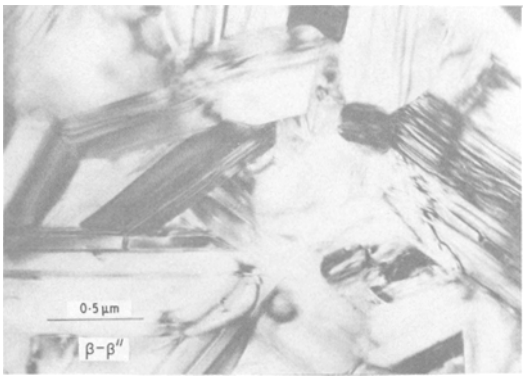

Figure 5 Transmission electron micrograph of as-sintered electrolyte.

resistivity of about 12 Ω cm†. It is immediately apparent that most of the grains are strongly faceted. Electron diffraction shows readily that this faceting is parallel to the conduction planes. In Fig. 6, this point is more clearly illustrated by a tracing of Fig. 5, in which all (0 0.1) faceted boundaries are represented by solid lines, and all general boundaries are shown as dashed lines. This is a feature that is common to all β and β''-aluminas and probably results from a particular grain growth mechanism operating during solid state sintering. The growth mechanism seems to be one in which whole spinel blocks propagate as ledges along the basal planes. Evidence for this may be seen in the high resolution lattice images of spinel block ledges that can be found along the (0 0.1) facets of the β-alumina grains [10]. It also suggests that the observation of strong facets does not necessarily imply the presence of liquid phases during sintering. The aspect ratio of a grain resulting from grain growth will simply depend on the nucleation rate of new spinel blocks on the (0 0.1) facets, compared to their rate of propagation. It is therefore to be expected that aspect ratios will depend sensibly on sintering or post-annealing treatment temperatures [11]; there are some indications that lower aspect ratios are obtained at lower sintering temperatures [12]. Fig. 7 shows a (0 0.1) facet grain boundary in detail. The lattice fringes are (0 0.2) fringes and can be thought of as representing spinel blocks. Na^+ transport through such grain boundaries must be negligible at temperatures around 300° C since the anisotropy of the diffusion coefficient is extreme. Such boundaries have to be considered as fully

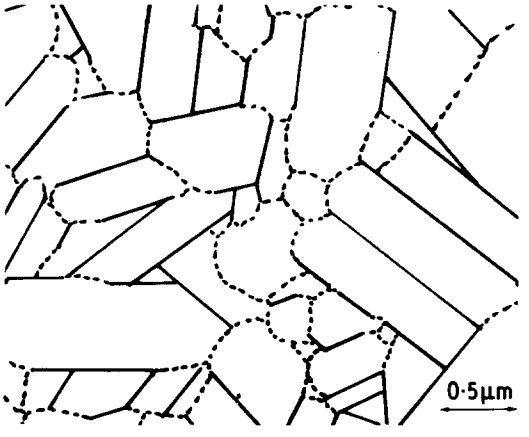

Figure 6 Tracing of grain boundaries in Fig. 5; solid lines (0 0.1) facets; dashed lines general boundaries.

blocking to sodium transport. In three dimensions, under d.c. flow conditions, the Na^+ would have to detour to reach another grain, as shown qualitatively in Fig. 8. These (0 0.1) faceted boundaries thus are not only intrinsically very blocking, but also screen part of the adjacent bulk from full participation in d.c. conduction. The preponderance‡ of the (0 0.1) facets makes it necessary to include their effect in quantitative considerations of d.c. ionic conduction in polycrystalline electrolytes. It is interesting to note here that if the microstructure were isomorphically enlarged, the effect of the blocking (0 0.1) grain boundaries would be to screen a constant fraction of the grain bulk from full participation in d.c. conduction. In a realistic grain growth situation the presence of the blocking grain facets is thus to reduce the in-

†G. May of Chloride Silent Power, Ltd., is thanked for providing this material.

‡ In thin sections used for transmission electron microscopy, the ratio of lengths of (0 0.1) faceted boundaries to other boundaries is about 1.

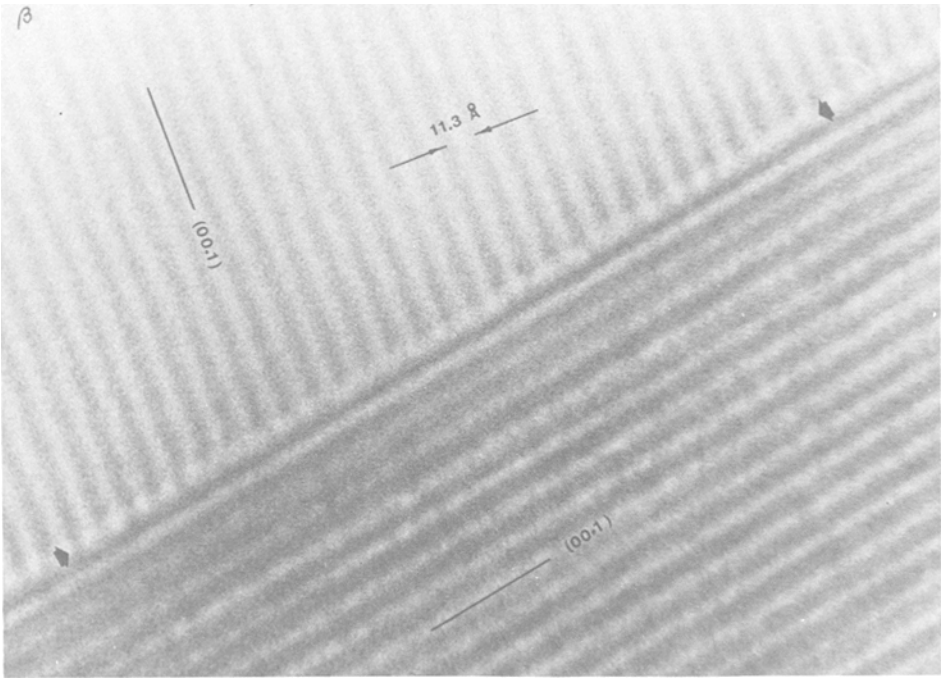

Figure 7 Lattice image of (0 0.1) facet blocking grain boundary.

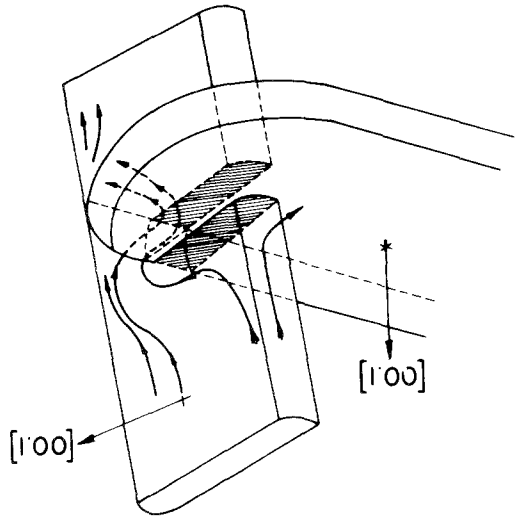

Figure 8 Three dimensional sketch of a grain intersection. The shaded areas are the highly blocking (0 0.1) facets. The current path is indicated qualitatively.

crease in ionic conductivity derived from grain growth upon post-annealing. Analogue experiments with conducting paper in which the blocking (00.1) facet grain boundaries of Fig. 6 were inscribed showed that the in-plane resistivity was increased by a factor of 2 compared to a "grain boundary free" analogue. This demonstrated that the faceting is indeed responsible for a non-negligible part of the total electrolyte resistivity. This suggests that it may be desirable to produce electrolytes with low aspect ratio grain morphologies.

At the other end of the grain boundary resistivity scale one can consider low angle grain boundaries with various habit planes. Low angle boundaries can frequently be found in sintered β-aluminas. These simple tilt boundaries are made up of dislocations with a Burgers vector of $\frac{1}{2}[c_0]$, i.e., 1 spinel block long [13]. Both the observation of spinel block ledges on (0 0.1) facets and of dislocations with $\mathbf{b} = 11.3\,\text{Å} = \frac{1}{2}[c_0]$ suggests strongly that the spinel blocks in β-aluminas are sturdy building blocks in which stacking faults involving the oxygen sublattice are energetically quite unfavourable. Low angle tilt boundaries should have little effect on the macroscopic ionic resistivities, though they may cause microscopical current concentrations that under unfavourable conditions may assist in electrolyte breakdown [14].

The low angle grain boundaries and the (0 0.1) facets present two extremes of grain boundary resistivities, for simple geometrical relationships. More generally, grain boundaries should be considered in the framework of Bollmann's geometrical treatment [15]. The grain boundary structure is primarily determined by the translation lattice of

the crystals between which the boundary exists. Consequently, as far as DSC dislocations [15–17] are concerned, the intrinsic grain boundary structure may not be as complicated as thought at first since the DSC structure should be independent of the complexity of the crystal basis. Other dislocations may, however, appear in grain boundaries when special local atomic arrangements are preferred [18]. Such arrangements would include in covalent crystals the preservation of, for example, tetrahedral bond angles [19], or in ionic crystals the preservation of octahedral or tetrahedral interstices. The result is that the grain boundaries can be made up of dislocations that are either total or partial DSC dislocations. At all times, however, the grain boundary structure must still be an event in the DSC lattice. Beta aluminas seem to be materials in which large DSC dislocations can occur due to the peculiarity that the spinel blocks seem to behave as structureless "jellium" layers that attempt to be in near registry with each other. This phenomenon should have important consequences for the grain boundary intergranular resistivities, and is described further below.

2.2.2. Simple tilt boundaries

Some simple tilt boundaries were referred to in the previous section. Fig. 9 shows another type of simple symmetrical tilt boundary. Here the boundary habit plane bisects the two $[c_0]$ directions ($\psi = 0$ in Fig. 10); the angle θ_c between the two $[c_0]$ directions is 19°. The diffraction conditions were such that two identical systematic and symmetrical 0 0*l* sets were operating in each grain.

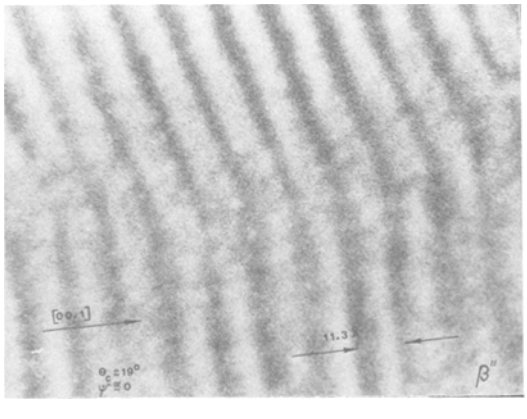

Figure 9 19° symmetrical tilt boundary.

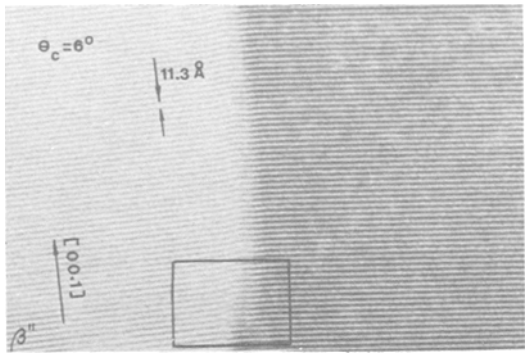

Figure 10 (a) Low angle 6° tilt boundary. Note the continuity of the lattice fringes across the boundary. The lattice fringes appear continuous before and after a dislocation-like feature (probably an inclined dislocation) in this boundary in the boxed area.

Seven beams of each crystal were used to form the image in axial illumination. The fringe shifts due to defocus should therefore be the same in both lattices [20], leading to the interpretation that the two lattices at such boundaries, where no strain contrast is evident, are very nearly in registry. The imaging geometry of these boundaries is not easily found in the random, polycrystalline electrolytes, but observations of this type on other tilt boundaries, such as the 6° tilt boundary shown in Fig. 10, tend to present the same aspects* regardless of rotations around $[c_0]$. The observations would then indicate that actual lattice displacements from the ideal coincidence site lattice across a grain boundary are of the order of fractions of oxygen interplanar spacings. This, together with the existence of dislocation with a Burgers vector of 11.3 Å $= \frac{1}{2}[c_0]$, led to considering the spinel blocks as structureless layers of "jellium" for which orientational mismatch can be accommodated in part by dislocations with Burgers vectors of strength $\mathbf{b} = \frac{1}{2}[c_0]$. This allows a much more simplified description of the important structural features of β- or β''-alumina grain boundaries. The structure of symmetrical or asymmetrical tilt boundaries is then readily described with the aid of Fig. 11. Where the "jellium" planes overlap a line of best fit or of minimum strain (MS) is present [21]. Relaxation would take place starting from these regions to form screw dislocations with $\mathbf{b} = \frac{1}{2}[c_0]$. The moiré fringes in Fig. 11 can thus be considered to be lines of constant Burgers vector. Clearly the

*Detailed dynamical calculations need to be performed, however, before such images, in which the diffraction conditions are not ideally symmetrical, can be reliably interpreted.

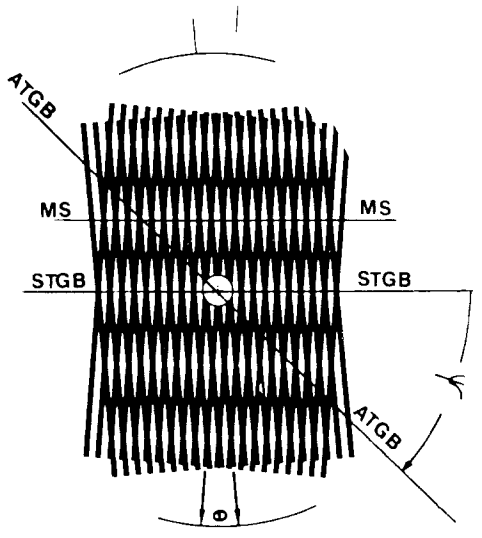

Figure 11 Geometry of symmetrical tilt grain boundary (STGB) as asymmetrical tilt grain boundary (ATGB) for a simple 0 0.1 tilt orientation, if the spinel blocks are treated as structureless continuum. MS: lines of minimum strain [21].

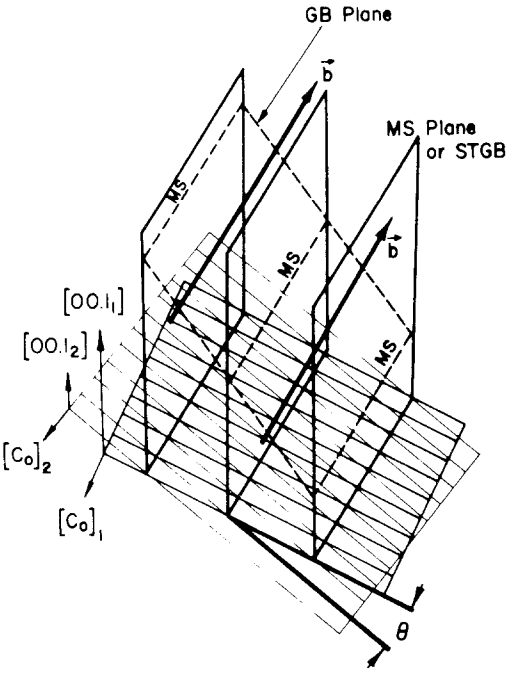

Figure 13 Three dimensional sketch of inclined boundary, GB plane, in simple 0 0.1 tilt oriented grains. MS: planes of "minimum strain". **b**: screw dislocations accommodating the twist component.

symmetrical tilt boundary (STGB in Fig. 11) will not contain dislocations, while the asymmetrical tilt boundary (ATGB) contains dislocations of strength $\mathbf{b} = \frac{1}{2}[c_0]$ where it is intersected by the moiré fringes. An example of an asymmetrical tilt boundary and its interpretation in these terms is shown in Fig. 12. The correspondence is evident.

2.2.3. Simple tilt and twist boundaries

A twist component has to be accommodated in simple tilt orientation relationships when the grain boundary habit plane is as shown in Fig. 12. The MS lines now become MS planes. The dislocations that would accommodate this twist component would be found as indicated in Fig. 13. In the electron microscope one will observe the projected image of this structure making verification of the dislocation spacings simple. A pure tilt boundary is shown projected in Fig. 14a. If $\frac{1}{2}[c_0]$ screw dislocations were to accommodate the twist, then a lattice image approaching that of Fig. 14b should be observed. If the habit plane of a simple (0 0.*l*) tilt boundary is not too steeply inclined to the thin foil surface, then one might hope to observe a lattice image geometry that resembles Fig. 14b for relaxed boundaries. Such a geometry corresponding to Fig. 14b is shown in Figs. 15a and b for a 6° simple tilt relationship. The images can be interpreted in this low tilt case, without ambiguity as to whether the grain boundary features

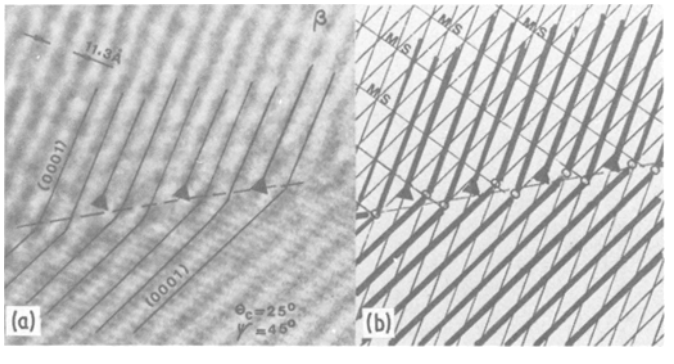

Figure 12 Asymmetrical tilt boundary: (a) lattice image (11.3 Å spacing); (b) corresponding geometry of simplified model.

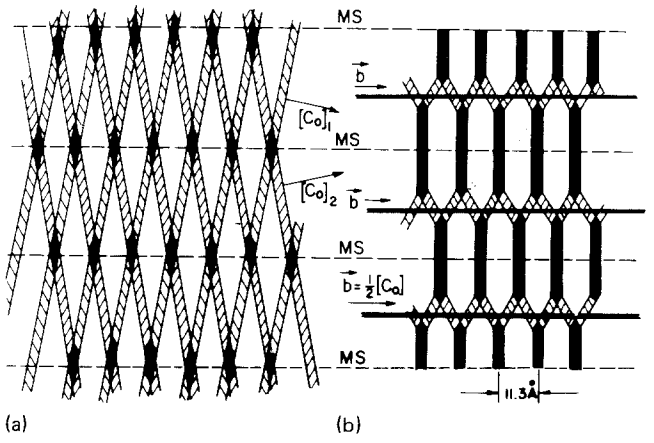

Figure 14 (a) Projected unrelaxed pure twist boundary. The dark areas are the "non-blocking sites", NB, where Na^+ transport is easy. The shaded areas are the blocked sites, B, where direct intergranular sodium transport is difficult. (b) Projected relaxed twist boundary, with accommodation by screw dislocations with $\mathbf{b} = 1$ spinel block.

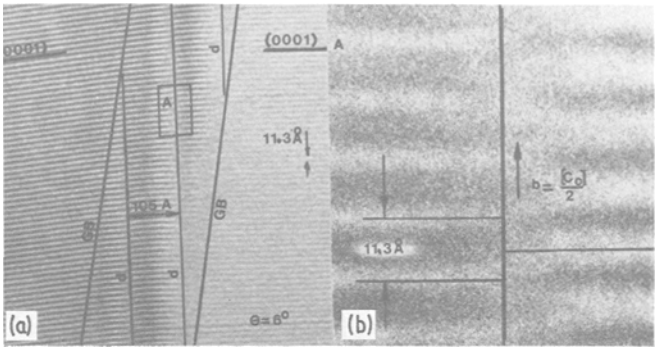

Figure 15 (a) Low angle twist orientation with grain boundary inclined as shown qualitatively in Fig. 13. The spacings of the dislocations, d, are as expected. (b) High magnification of area A. The observed lattice fringe geometry resembles Fig. 14b.

are moiré fringes or screw dislocations. The dislocation marked "a" in Fig. 15a and shown in more detail in Fig. 15b is indeed a screw dislocation with $\mathbf{b} = 11.3$ Å. Note that Fig. 15b also seems to indicate that the core "width" of the dislocation is of the order of $b = \frac{1}{2}[c_0]$. For higher simple tilt orientation relationships the screw component gets larger in the geometry of Fig. 12, the screw dislocations get closer together and become more difficult to distinguish from moiré fringes. With sufficiently higher tilts and strong twist components, the screw dislocations eventually should be too close together, so that spinel block matching by means of $\mathbf{b} = \frac{1}{2}[c_0]$ dislocations become energetically unfavourable due to extensive dislocation core overlap. It thus can be reasonably postulated that at some point dislocations with the large Burgers vector will no longer be able to accommodate the grain boundary mismatch and the boundary would consist totally of DSC dislocations with very small Burgers vectors. Fig. 16 is believed to show such a case where only moiré fringes M are superimposed on the lattice images. The structure of such higher angle boundaries would thus resemble much more closely the structure of an unrelaxed boundary.

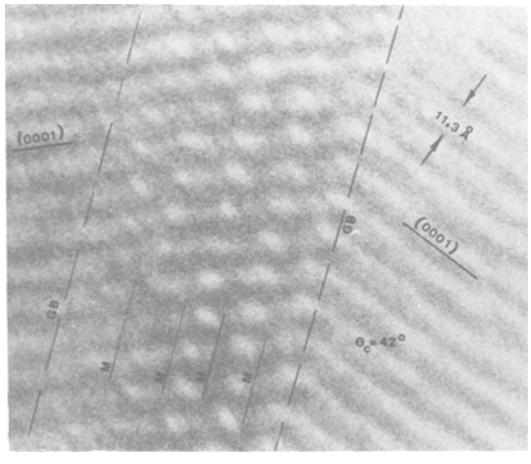

Figure 16 Inclined grain boundary in 42° simple tilt 0 0.1 tilt geometry. The grain boundary features, M, are interpreted as moiré fringes.

The significance of the possibility of accommodating grain boundary mismatch with Burgers vector of magnitude 11.3 Å is that the ratio of blocking/non-blocking sites in the β-alumina grain

boundaries, B/NB, is substantially decreased. The detailed nature of the non-blocking, or less blocking, site is at present unknown. It will depend on the magnitude of the offset from the ideal spinel block matching referred to in Section 2.2.2. In the most favourable case of a pure twist boundary, Fig. 14, the non-blocking sites would approach the bulk environment. In case small shifts from the perfect CSL positions occur, one would expect that the grain boundary contribution to the sample resistivity would proportionately increase compared to the bulk resistivity with increasing radius of the transported ion. Experiments on Na-β-aluminas substituted with Ag^+ and with the smaller Li^+ are in progress. The details of these experiments will be reported later. Assuming that the grain boundary screw dislocations have a blocking core width about equal to their Burgers vector, $\frac{1}{2}[c_0]$ as suggested by Fig. 15, then a comparison of the B/NB grain boundary site ratio is easily made in the simple (0 0.1) twist case. The switch-over to orientation independent grain boundary resistivity, based on a simple geometrical argument, would occur at a twist misorientation between 40° and 45° as shown in Fig. 17. This is a substantial misorientation, and a large number of grain boundaries may therefore be expected to have a structure in which twist mismatch is accommodated by the $\frac{1}{2}[c_0]$ screw dislocation.

It can be reasonably assumed that the temperature independent factor of intergranular grain boundary resistivity is roughly proportional to the ratio of blocking to non-blocking sites. Additionally, if in a.c. measurements grain boundary capacitance would be of the inner layer type, it would be equally plausible that the grain boundary capacitance would also be proportional to the blocking/non-blocking site ratio. The temperature independent factor of grain boundary resistivity and the grain boundary capacitance should therefore be proportional to each other.

It is clear then from these observations and considerations that sodium beta alumina contains a wide range of grain boundary structures and consequently a wide range of intergranular grain boundary transport properties. Sodium beta alumina solid electrolytes are therefore non-homogeneous, anisotropic conductive media. This is the basis of the difficulty interpreting the a.c. dispersive measurements in detail, as discussed later.

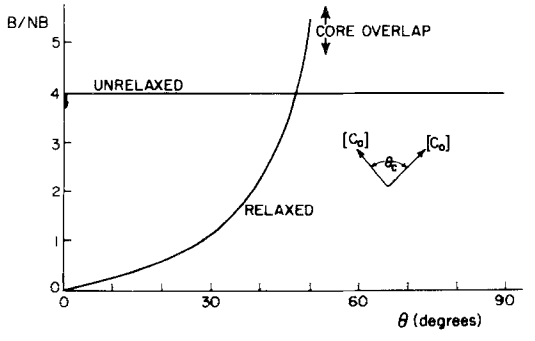

Figure 17 Ratio, B/NB, of blocking sites B, to non-blocking sites NB, for unrelaxed and relaxed pure *h k*.0 twist boundary.

2.3. Dirty grain boundaries

Practical ceramics invariably contain impurities which potentially affect their properties. β-aluminas are no exception and their grain boundaries in particular may be susceptible to impurity segregation, or intergranular phase formation. We have investigated the effects of a variety of impurities including Si and Ca on the ionic conduction properties of β-alumina [22, 23]. The presence of Si leads to the formation of sodium-aluminosilicate intergranular phases, which at levels above 0.5 wt% SiO_2 can be readily detected by electron microscopy. Below this level, the sampling statistics of the transmission electron microscope are unfavourable for detection. The silicates were found to collect intergranularly, preferably at triple junctions. Occasionally the silicate phase penetrated well between the grain boundaries, but this was not generally the case [22]. One thus deals with grain boundaries which are at least partly free of a second, low ionic conductivity phase, as well as with grain boundaries containing second phase intergranular material of a widely varying thickness. Clearly the grain boundaries are not uniformly affected; rather an increasing fraction of grain boundaries can be expected to behave in a highly blocking fashion if more silicate is present. There is no evidence that silica has any measureable solubility in beta alumina, so at low impurity levels (below 0.1 wt% SiO_2) the effects of Si contamination on ionic resistivity is difficult to measure in β-alumina since it probably will be accommodated in isolated second phase pockets leaving most grain boundaries unaffected.

The case of Ca is more complex than that of Si. Ca^{2+} can substitute for Na^+ if additional O^{2-} is

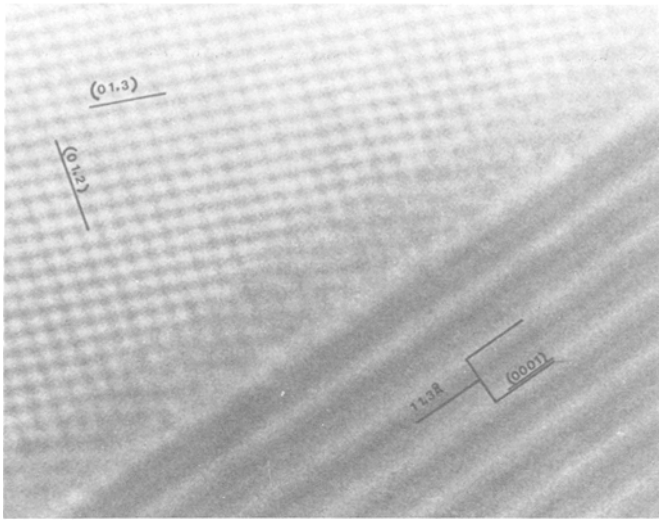

Figure 18 Disturbed lattice fringes at grain boundary in Ca-containing electrolyte.

incorporated [3]. Additionally, liquid phases in the system Al_2O_3–CaO–Na_2O are readily formed at sintering temperatures (typically 1750° C). Solid solution entails the possibility of formation of impurity atmospheres at grain boundaries. When significant levels of CaO are present (~ 0.5 wt% CaO) fracture modes change from mainly transgranular to mainly intergranular. Then Auger spectroscopy can be used to detect possible grain boundary impurity accumulation. Using this technique Unertl *et al.* observed such accumulations in a region of about 200 Å at the fracture surfaces of Ca-doped β-aluminas [24]. This is evidence that Ca can indeed accumulate at grain boundaries, either as a solid solution atmosphere, or as a very thin uniform intergranular phase. Transmission electron microscopy revealed disturbed lattice fringes at some grain boundaries, Fig. 18. While it is tempting to see this as evidence of impurity accummulation at grain boundaries, the interpretation of the image has to remain somewhat ambiguous in the absence of a direct local chemical analysis. More importantly, electron microscopy also revealed the presence of an intergranular $CaO \cdot 6\,Al_2O_3$ (C6A) phase with a geometry which indicates it was liquid at one point during the sintering. Fig. 19 shows such a C6A phase. The phase extends well along low angle grain boundaries, as shown in the bright field (a), and dark field (b) images in Fig. 20. Lattice imaging at the tip of this phase, Fig. 21, indicates that, contrary to the silicate case, a normal low angle dislocation grain boundary seems to be established. The C6A phase seems to be found preferentially between such grain geometries. It is possible that the reason for such behaviour is to be sought in different reaction kinetics between β-alumina and calcium-(sodium)-aluminates at different types of interfaces; e.g., a (0 0.1) facet is likely to be a slow kinetics interface.

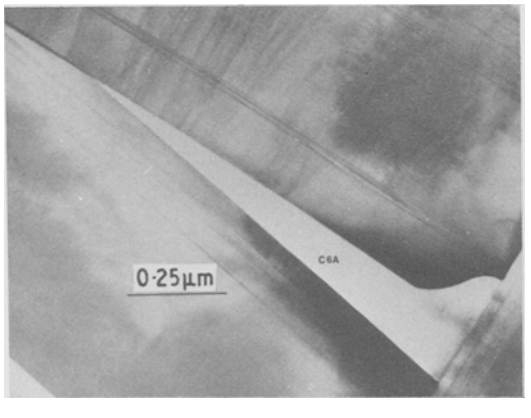

Figure 19 Second phase $CaO \cdot 6\,Al_2O_3$ (C6A) phase in Ca-containing electrolyte. The shape of the second phase suggests it was liquid at one point during sintering.

3. A.c. dispersive measurements and critique of simple equivalent circuits

In virtually all dielectrics, a dispersion of dielectric constants can be observed that deviates from ideal Maxwell behaviour. β-aluminas are no exception to this. Their dispersion of complex impedance or admittance has, however, been interpreted with a rather simplified equivalent circuit in which an ideal resistor representing the grain bulk is in

series with an ideal leaky capacitor representing the grain boundaries [5, 6]. A.c. measurements thus allow, according to this circuit, a straightforward separation of transgranular and average lumped intergranular resistivities, Fig. 22. Parameters such as grain bulk and grain boundary resistivity and activation energies, as well as grain boundary capacities are then reported and analysed in some detail. Some conductivity data based on this present model are shown in Fig. 23. It is clear that the grain boundary resistivity activation energy increases with temperature and at lower temperatures tends towards the bulk activation energy. Similar observations were made, e.g., by Lilley *et al.* [25]. The lumped grain boundary capacitance increases with increasing temperature as shown in Fig. 24. Some typical admittance data as a function of temperature are shown in Figs. 25a, b, c and d. Clearly there is a significant deviation from the ideal behaviour suggesting a wide spread in relaxation times [26].

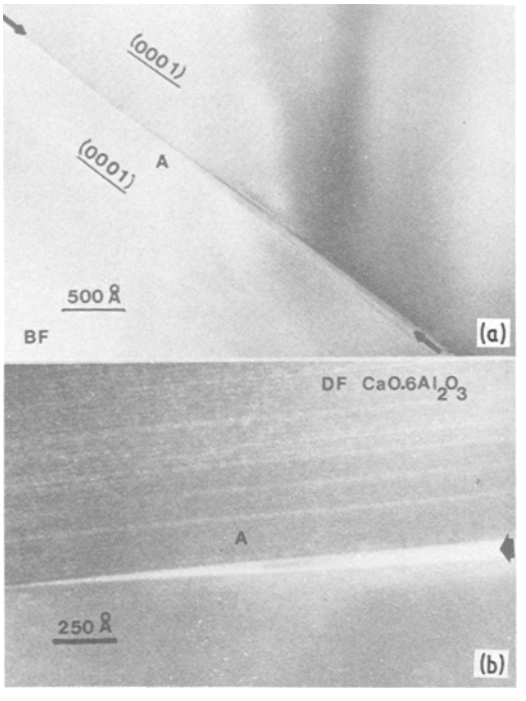

Figure 20 (a) Bright-field image of $CaO \cdot 6\ Al_2O_3$ (C6A) intergranular phase. (b) Dark-field image of $CaO \cdot 6\ Al_2O_3$ intergranular phase.

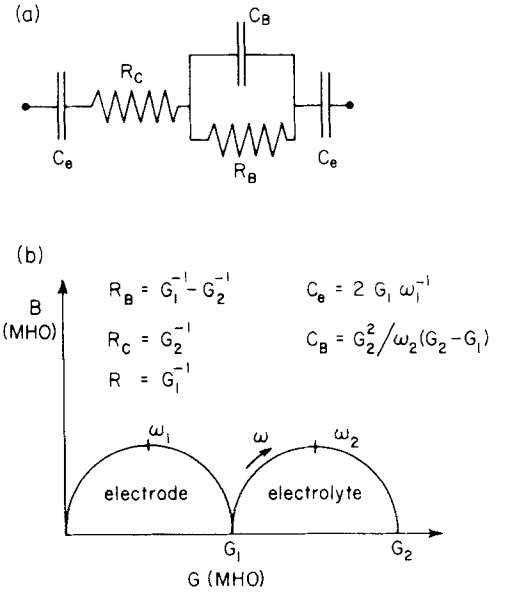

Figure 22 Simplified equivalent circuit and response in complex admittance plane (*B–G*).

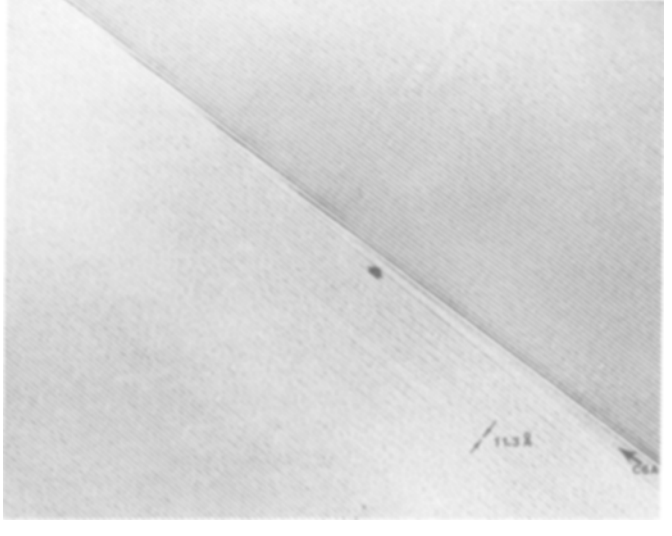

Figure 21 Lattice image showing transition from intergranular $CaO \cdot 6\ Al_2O_3$ (C6A) phase to an apparently normal low angle tilt boundary.

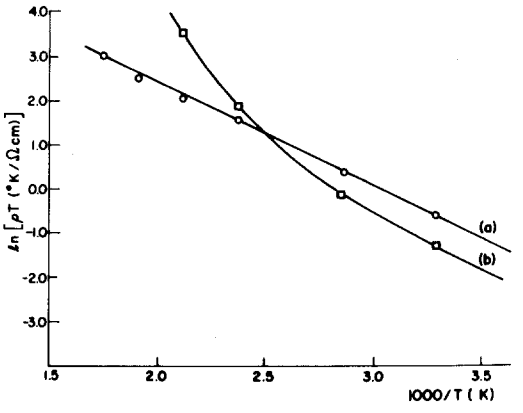

Figure 23 Grain bulk (a) and grain boundary (b) conductivity data of sodium beta alumina polycrystal, based on simplified equivalent circuit shown in Fig. 22.

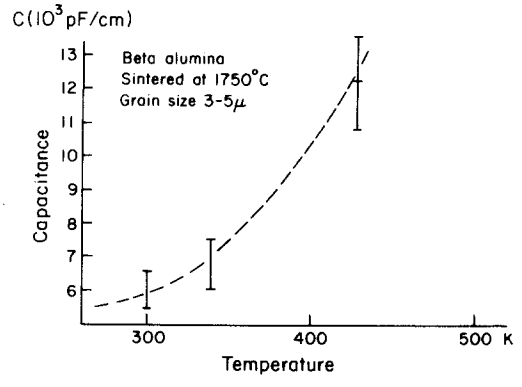

Figure 24 Lumped grain boundary capacitance, C_B in Fig. 22, as a function of temperature.

The question arises as to what degree the data can reveal meaningful information about some average grain boundary relaxation process. Below it is argued that the microstructure and wide spread in grain boundary ionic transgranular resistivities introduce significant complications that make the dispersive data, at present, non-interpretable in a physically meaningful way.

3.1. Series approach

The simplest way to explain the spread in relaxation times, and to interpret the high and low frequency intercepts, either in the complex impedance or complex admittance plane, is to argue that on the average all current paths will be identical. This leads to a series circuit as shown in Fig. 26 which in the simple interpretation would be reduced to the equivalent circuit of Fig. 22. In the complex impedance plane from the frequency ω_m at which $X(\omega)$, the reactance, is maximum, the average relaxation time $\bar{\tau}$ is found. If we have N grains in series then $R_B = \sum_i^N R_i$ and $R_c = \sum_i^N R_{c_i}$, where $N \equiv (\text{grain size})^{-1}$. This would simply lead to the average values $\bar{R}_{B_i} = R_B/N$ and $\bar{R}_{c_i} = R_c/N$. The grain boundary capacitance is easily shown to be $C_B = (\omega_m R_B)^{-1}[(R_c + R_B)/R_c]^{1/2}$ so that $\bar{C} \cong NC_B$ where $\bar{C}$ = average capacitance associated with an average single grain boundary. With this approach at room temperature for our samples we typically find an average capacitance of

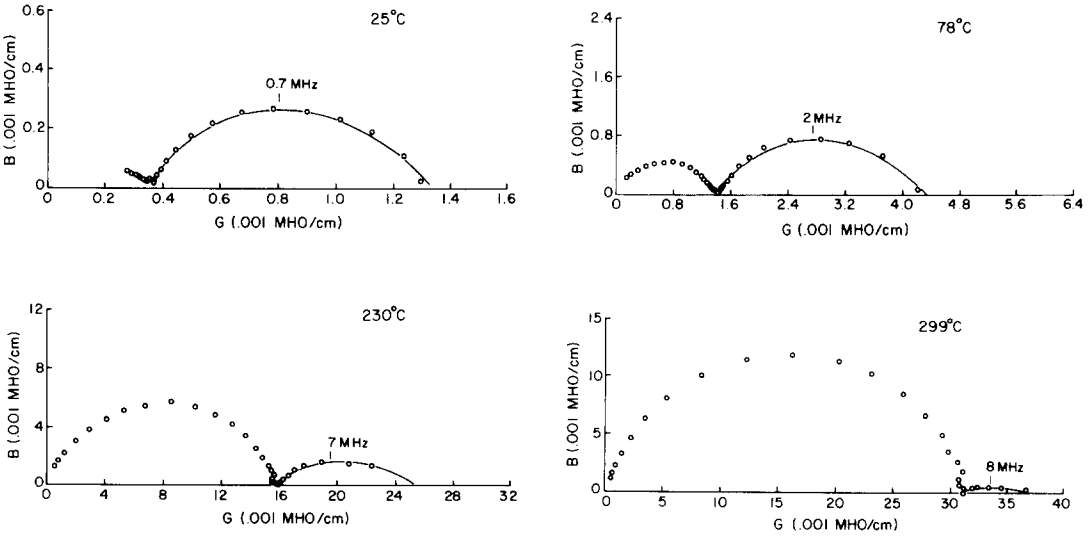

Figure 25 Typical complex admittance data on as-sintered sodium beta alumina sample at various temperatures. The frequency at which B_{max} occurs is indicated.

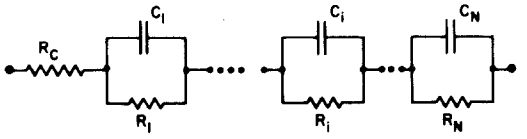

Figure 26 Simple series multi-element equivalent circuit.

$C \cong 1\,\mu F\,cm^{-2}$ of grain boundary, and an average resistance of $R_i \simeq 2\,\Omega\,cm^{-2}$ of grain boundary.

These values can only be considered approximate since it will be demonstrated that the series approach is not valid in detail. The values of the capacitance were independent of the a.c. r.m.s. voltage drops between 1 mV and 30 V per cm over the sample. Diffuse double layer capacitances would in this range be expected to be voltage dependent [27]. Both the observation of voltage independent capacitances, and the consideration that the calculated Debye lengths for diffuse double layers for these electrolytes are physically meaningless (i.e., less than 2 Å) supports the conclusion that the capacitances are of the inner layer type. They thus may be linked simply to the grain boundary structure, that is to the ratio of blocking/non-blocking sites. It should be noted that the difference between high and low frequency limit conductivities in the B–G (susceptance–conductance) or R–X (resistance–reactance) plots indeed yields a meaningful average "grain boundary" or intergranular resistivity if the series approach were valid.

3.2. Parallel approach

It was clearly demonstrated in Section 2 that we have to expect a wide range of intergranular resistivities in β-alumina solid electrolytes, so that *every* grain will be bounded by grain boundaries that statistically have a wide spread in intergranular resistivities. This has as a consequence that one must consider the ionic d.c. current flow to be non-homogeneous. An identical way of stating this is that the complete equivalent circuit of the ceramic solid electrolyte contains current paths which have different inter-electrode resistivities. The sodium ion current then distributes itself such that low resistivity paths, containing many low resistivity grain boundaries, are favoured over high resistivity paths so that not all grain boundaries carry the same current. Since the grain boundaries should generally have a higher activation energy for intergranular Na^+ transport than the bulk material, the current should become more homogeneous as the ratio grain boundary resistivity/bulk resistivity decreases, i.e., at higher temperatures.

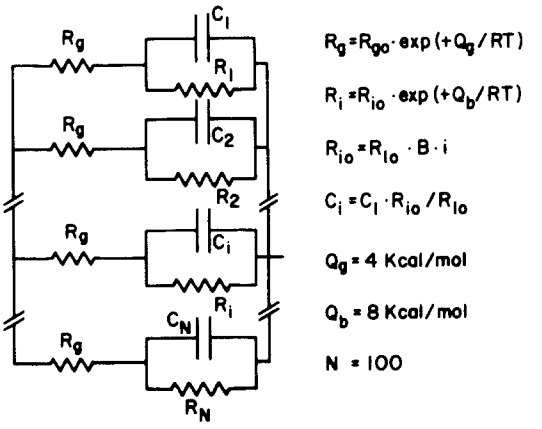

Figure 27 Simple parallel, multi-element equivalent circuit.

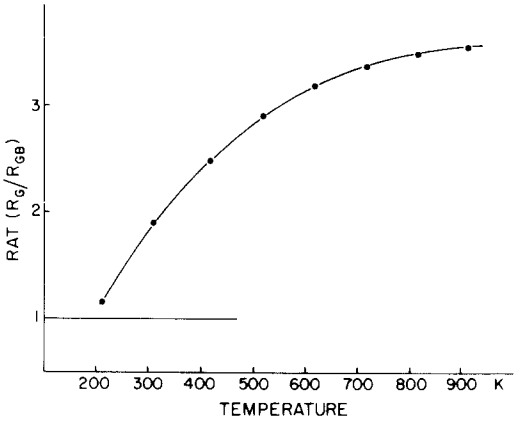

Figure 28 R_B/R_{GB} computed for parallel model shown in Fig. 27.

It is useful to consider the effects of these current inhomogeneities by modelling the electrolyte with a purely parallel equivalent circuit, rather than a series one. The essentials of this consideration were recently reported by Hsieh and De Jonghe with a simplified circuit of two parallel branches [22]. A more elaborate circuit containing 100 parallel elements was examined here, as shown in Fig. 27. All bulk grain resistivities R_g are taken identical; the intergranular capacitances, C_i, were set proportional to the temperature independent parts, R_{io}, of the grain boundary resistance, R_i, as suggested by the considerations in Section 2.2.3. The values are indicated in Fig. 27. The apparent lumped capacitance C_B and the apparent lumped grain boundary resistance R_B were then computed on the basis of the model in Fig. 22. Since the values of the grain boundary resistance should be independent of the bulk

resistance, it is easy to find the "true" lumped grain boundary resistance, R_{GB}, of the model by putting $R_g = 0$; $R_{GB} = (\Sigma_i R_i^{-1})^{-1}$.

R_B/R_{GB} was found to deviate significantly from 1. The amount of the deviation depends on the spread in the ratio of R_i/R_g. The results of the computation are shown in Fig. 28. The basis of the discrepancy is that the apparent lumped grain boundary resistivity R_B in such a circuit actually contains also parts of the bulk resistivity [22]. The current distribution gets progressively more inhomogeneous at low temperatures, so that a large amount of current flows preferentially through low resistivity paths. The result is that the apparent activation energy for intergranular transport will tend to lower values at lower temperatures. This effect is indeed observed in the actual ceramic electrolyte.

The computed lumped grain boundary capacitance C_B comes out to be temperature dependent as well, although each individual C_i was temperature independent. The results of the computations are shown in Fig. 29, and reflect qualitatively the actually observed lumped intergranular capacitance behaviour as a function of temperature.

The calculations on the circuits made of parallel components thus illustrate that the procedure of subtracting high frequency resistivity (bulk) from low frequency or d.c. resistivity does not yield a resistivity that may legitimately be called the "intergranular resistivity". Only when the intergranular resistivity totally dominates the sample resistance (i.e., at low temperature) is $R_B = R_{GB}$. It should, however, be noted that at low temperatures the lumped grain boundary resistance is some average that favours low resistivity boundaries. Unless the real equivalent circuit is somehow determined, it is difficult to interpret this average.

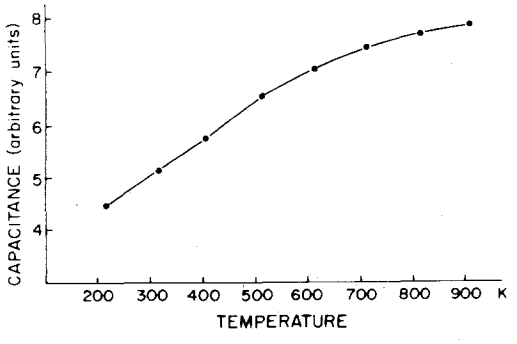

Figure 29 C_B, lumped grain boundary capacitance as in Fig. 23, computed as a function of temperature for parallel model as shown in Fig. 27.

The detailed study of the apparent intergranular transport activation energy of polycrystalline electrolyte is consequently of little physical significance, especially when R_C becomes comparable to R_B.

3.3. Mixed circuit approach

Some limited mixed circuits have also been studied [28]. The results again indicate the failure of the simple equivalent circuit interpretation, and the main conclusions are analogous to that of the pure parallel case.

3.4. A.c. ionic resistivities of electrolyte containing grain boundary phases

It was reported in the Section 2.3 that second phases such as sodium–alumino–silicates and calcium aluminates do not cover grain boundaries uniformly. Interestingly, the 300° C d.c. resistivities in both cases follow a relationship of the type $\log R = A + Bx$ where R is the 300° C resistivity, A and B are constants, and x is the amount of the second phase [22, 23]. Thus the two-phase electrolytes with grain boundary phases seem to obey the "logarithmic mixing rule" behaviour [28, 29]. The behaviour of the grain boundary capacitances for such electrolytes is interesting: C_B strongly decreases with increasing per cent of second phase, as shown in Fig. 30. It is tempting to interpret this phenomenon as a simple decrease in the geometrical capacitances now arising at grain boundaries due to a uniform, poorly conducting second phase of increasing thickness. The inhomogeneity of the second phase distributions as demonstrated in Section 2.3 does not permit such a simple interpretation. It is suggested that the observation of a

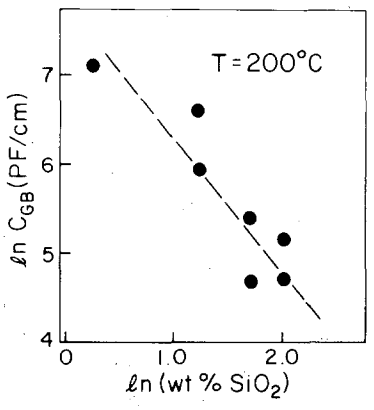

Figure 30 C_B versus wt% SiO_2 in silicate-containing electrolyte.

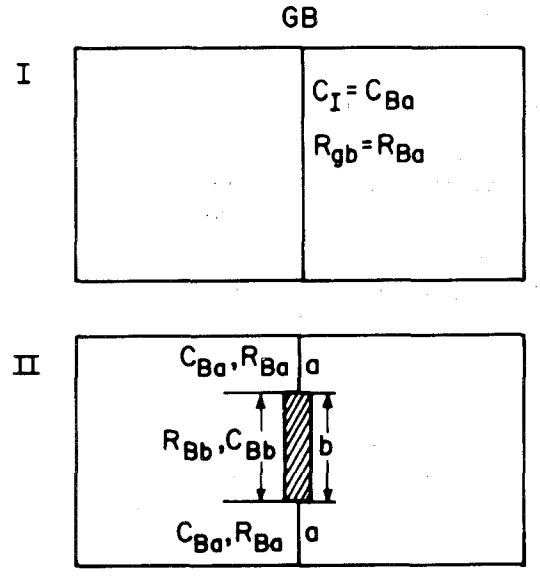

Figure 31 Simple geometry of non-conducting, partially covering grain boundary phase.

decreasing apparent grain boundary capacitance can also be explained qualitatively on the basis of partial coverage of the grain boundaries by a poorly conducting phase, as depicted schematically in Fig. 31 for a hypothetical 1-grain boundary sample. Let A be the area of the clean grain boundary with $R_B = R_{gb}$ and $C_B = C_I$. Now consider the grain boundary in case II, being clean at "a" and containing a second phase at "b", then at "a".

$$R_{Ba} = R_{gb}$$

$$C_{Ba} = C_I$$

while at "b":

$$R_{Bb} \gg R_{gb}$$

$$C_{Bb} = (1/C_I + 1/C_{geom})^{-1}$$

where

C_{geom} = the geometrical capacitance associated with the second phase at b.

For any significant thickness of the second phase, we would expect

$$C_{geom} \ll C_I \quad \text{so that} \quad C_{Bb} \cong C_{geom}$$

So in case II, the total grain boundary resistance

$$R_{B_{II}} \cong R_{gb}(A/A_a)$$

where A_a = total area of type "a" grain boundary.

At the same time, the total grain boundary capacitance

$$C_{B_{II}} = C_I(A_a/A)$$

since $C_{geom} \ll C_I$.

The average relaxation time determined by the product $C_{B_{II}}R_{B_{II}}$ will therefore not vary significantly from the "clean" case, i.e., $\tau_I \cong \tau_{II}$, or the frequency, ω_m, at which the maximum in X occurs in the complex impedance plane will not be affected significantly so that

$$C_{B_I} = (\omega_m \cdot R_{B_I})^{-1}\,[(R_c + R_{B_I})/R_c]^{1/2}$$

$$C_{B_{II}} = (\omega_m \cdot R_{B_{II}})^{-1}\,[(R_c + R_{B_{II}})/R_c]^{1/2}$$

and since $R_{B_{II}} < R_{B_I}$,

we have $C_{B_{II}} < C_{B_I}$.

It is thus not necessary to involve the realistic microstructural feature of uniform grain boundary coverage to account qualitatively for the decrease in the apparent grain boundary capacitance in the presence of non-homogeneously distributed second phase. Unfortunately, it seems at present rather difficult to work out a treatment taking the microstructure quantitatively into account.

All the considerations lead to the belief that little fundamental electrochemical information about grain boundaries can be extracted from a.c. dispersive measurements on polycrystalline ceramics. Rather one should aim to characterize single grain boundaries, e.g., in welded bicrystals. Such experiments are in progress in our laboratory. The a.c. characterization method, however, remains an invaluable tool to provide, easily and rapidly, engineering correlations between conductive properties, microstructures and compositions of the ceramic solid electrolytes.

4. Summary and conclusions

(1) Grain boundary morphology and structure has been examined in detail in sodium β-alumina solid electrolytes, and plausible correlations have been advanced, based on the detailed transmission electron microscopy, between the grain boundary structure and its resistivity and capacitance.

(2) The geometrical aspects and resistance of the grain boundary depend on whether or not screw dislocations with $\mathbf{b} = 1$ spinel block can accommodate orientational mismatch. Such dislocations have been observed for a number of grain boundaries.

(3) Second phases are generally distributed inhomogeneously in the electrolytes even if wetting angles are near zero.

(4) The wide spread in grain boundary resistivities and capacitances can account for the deviations from the ideal Maxwell dispersion behaviour. However, determination of physically meaningful equivalent circuit parameters from dispersive type measurements on polycrystals seems not possible at present. Several model circuits were used to illustrate the difficulties that the microstructural inhomogeneities introduce in the interpretation of the dispersive data.

Acknowledgements

This work was supported by the Electric Power Research Institute. Additional support was received from the National Science Foundation through the Cornell Materials Science Center. Discussions with R. Balluffi, D. Hewitt and E. Lilley are gratefully acknowledged. A. Buechele is thanked for experimental assistance.

References

1. G. E. YOUNGBLOOD, A. V. VIRKAR, W. R. CANNON and R. S. GORDON, *Ceram. Bull.* **56** (1977) 206.
2. J. B. BUSH, Principal Investigator, General Electric Company Research and Development Center; Electric Power Research Institute, RP 128-2 (1975).
3. J. T. KUMMER, *Prog. Solid State Chem.* 7 (1972) 141.
4. M. S. WHITTINGHAM and R. A. HUGGINS, *J. Electrochem. Soc.* **118** (1971) 1.
5. R. W. POWERS and S. P. MITOFF, *ibid.* **122** (1975) 221.
6. J. E. BAUERLE, *Phys. Chem. Solids* **30** (1969) 2651.
7. S. SARIAN, B. J. DUNBAR and W. J. McENTEE, "Ceramic Microstructures '76", edited by R. M. Fulrath and J. A. Pask (Westview Press, Boulder, 1977) p. 621.
8. A. V. VIRKAR and R. S. GORDON, *ibid.* p. 610.
9. L. K. H. VAN BEEK, *Progr. Dielectrics* 7 (1967) 69.
10. L. C. De JONGHE, *J. Amer. Ceram. Soc.* (to be published).
11. L. C. De JONGHE and E. GOO, 14th University Conference on Ceramic Science, November 1977, North Carolina State University (in press).
12. L. C. De JONGHE and E. GOO, unpublished data (1977).
13. L. C. De JONGHE, *J. Mater. Sci.* **11** (1976) 206.
14. *Idem. Scripta Met.* **10** (1976) 285.
15. W. BOLLMANN, "Crystal Defects and Crystalline Interfaces" (Springer–Verlag, Heidelberg, 1970).
16. *Idem., ibid.* p. 208.
17. R. W. BALLUFFI, Y. KOMEN and T. SCHOBER, *Surface Sci.* **31** (1972) 68.
18. R. C. POND and V. VITEK, *Proc. Roy. Soc.* **A 357** (1977) 453.
19. O. L. KRIVANEK, S. ISODA and K. KOBAYASHI, *Phil. Mag.* **36** (1977) 931.
20. D. J. H. COCKAYNE, J. R. PARSON and C. W. HOELKE, *Phil. Mag.* **30** (1971) 139.
21. W. BOLLMANN, "Crystal Defects and Crystalline Interfaces" (Springer–Verlag, Heidelberg, 1970) p. 122.
22. M. Y. HSIEH and L. C. De JONGHE, *J. Amer. Ceram. Soc.*
23. L. C. De JONGHE and A. BUECHELE, Cornell Materials Science Center Report #2428, April 1975.
24. W. N. UNERTL, L. C. De JONGHE and Y. Y. TU, *J. Mater. Sci.* **12** (1977) 739.
25. E. LILLEY and J. E. STRUTT, International Conference on Defects in Insulating Crystals, Gatlingburg, October 1977 (NTIS publication, 1977) pp. 266–7.
26. K. S. COLE and R. H. COLE, *J. Chem. Phys.* **9** (1941) 341.
27. DOUGLAS O. RALEIGH, "Electrode Processes in Solid State Ionics", edited by M. Kleintz and J. Dupuy (D. Reidel, Dordreht, 1976) pp. 119–47.
28. L. C. De JONGHE, Electric Power Research Institute, RP 252-2, July 1977.
29. D. A. PAYNE, "Ceramic Microstructures '76", R. M. Fulrath and J. A. Park (Westview Press, Boulder, 1977) pp. 584–97.

Received 13 February and accepted 25 April 1978.